nature energy

SUPPLEMENTARY INFORMATION

https://doi.org/10.1038/s41560-019-0538-4

In the format provided by the authors and unedited.

Managing grains and interfaces via ligand anchoring enables 22.3%-efficiency inverted perovskite solar cells

Xiaopeng Zheng[1,6], Yi Hou[2,6], Chunxiong Bao[3], Jun Yin[1], Fanglong Yuan[2,4], Ziru Huang[2], Kepeng Song[1], Jiakai Liu[1], Joel Troughton[1], Nicola Gasparini[1], Chun Zhou[2], Yuanbao Lin[1], Ding-Jiang Xue[2], Bin Chen[2], Andrew K. Johnston[2], Nini Wei[5], Mohamed Nejib Hedhili[5], Mingyang Wei[2], Abdullah Y. Alsalloum[1], Partha Maity[1], Bekir Turedi[1], Chen Yang[1], Derya Baran[1], Thomas D. Anthopoulos[1], Yu Han[1], Zheng-Hong Lu[4], Omar F. Mohammed[1], Feng Gao[3], Edward H. Sargent[2*] and Osman M. Bakr[1*]

[1]Division of Physical Sciences and Engineering, King Abdullah University of Science and Technology (KAUST), Thuwal, Saudi Arabia. [2]Department of Electrical and Computer Engineering, University of Toronto, Toronto, Ontario, Canada. [3]Department of Physics, Chemistry and Biology (IFM), Linköping University, Linköping, Sweden. [4]Department of Materials Science and Engineering, University of Toronto, Toronto, Ontario, Canada. [5]Imaging and Characterization Core Lab, King Abdullah University of Science and Technology (KAUST), Thuwal, Saudi Arabia. [6]These authors contributed equally: Xiaopeng Zheng, Yi Hou. *e-mail: ted.sargent@utoronto.ca; osman.bakr@kaust.edu.sa

Supplementary Information for

Managing grains and interfaces via ligand anchoring enables 22.3% efficiency inverted perovskite solar cells

Xiaopeng Zheng[1, †], Yi Hou[2, †], Chunxiong Bao[3], Jun Yin[1], Fanglong Yuan[2,4], Ziru Huang[2], Kepeng Song[1], Jiakai Liu[1], Joel Troughton[1], Nicola Gasparini[1], Chun Zhou[2], Yuanbao Lin[1], Ding-Jiang Xue[2], Bin Chen[2], Andrew K. Johnston[2], Nini Wei[5], Mohamed Nejib Hedhili[5], Mingyang Wei[2], Abdullah Y. Alsalloum[1], Partha Maity[1], Bekir Turedi[1], Chen Yang[1], Derya Baran[1], Thomas D. Anthopoulos[1], Yu Han[1], Zheng-Hong Lu[4], Omar F. Mohammed[1], Feng Gao[3], Edward H. Sargent[2, *], and Osman M. Bakr[1, *]

[1]Division of Physical Sciences and Engineering, King Abdullah University of Science and Technology (KAUST), Thuwal 23955-6900, Saudi Arabia.

[2]Department of Electrical and Computer Engineering, University of Toronto, 35 St George Street, Toronto, Ontario, M5S 3G4, Canada.

[3]Department of Physics, Chemistry and Biology (IFM), Linköping University, Linköping, Sweden.

[4]Department of Materials Science and Engineering, University of Toronto, 184 College Street, Toronto, Ontario M5S 3E4, Canada.

[5]Imaging and Characterization Core Lab, King Abdullah University of Science and Technology (KAUST), Thuwal 23955-6900, Saudi Arabia.

Supplementary Figure 1. Water contact angles for perovskite films with different alkyl chain length AALs. a-e, Water contact angles of the pristine CsFAMA film (**a**) and the CsFAMA film with BA (**b**), PEA (**c**), OA (**d**), and OAm (**e**).

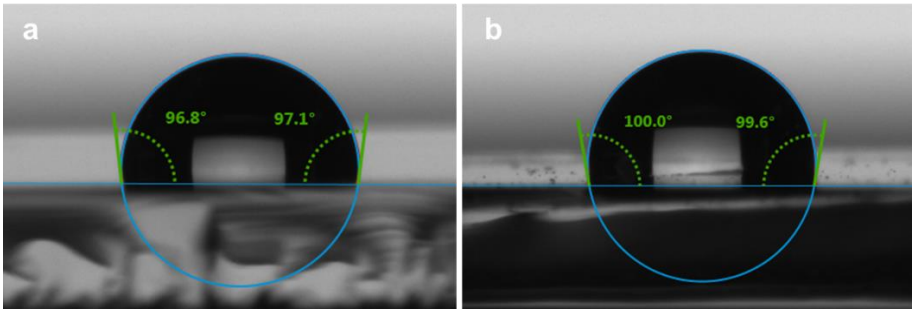

Supplementary Figure 2. AAL concentration dependent water contact angles. a, **b** Water contact angles of the CsFAMA film with 0.05 wt% AALs (OAm) and the CsFAMA film with 0.2 wt% AALs (OAm), respectively.

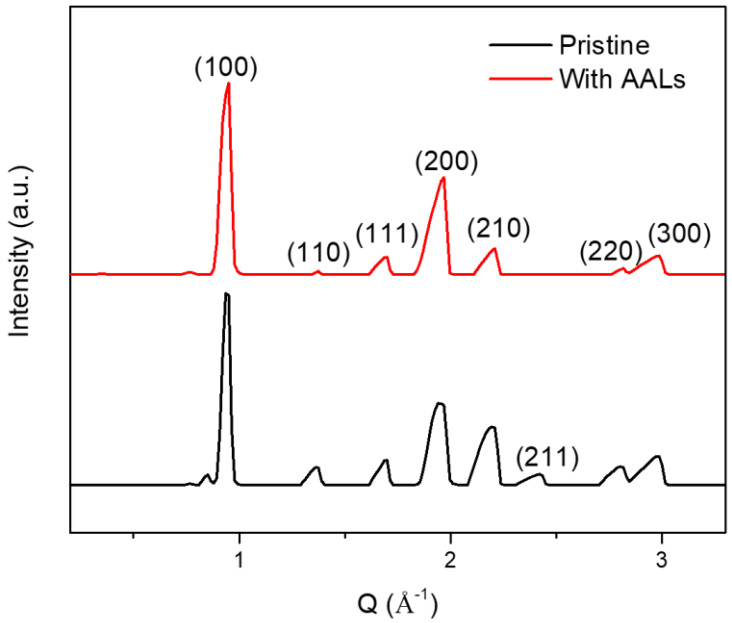

Supplementary Figure 3. Integrated intensity of GIWAXS data along q_z. Integrated intensity of GIWAXS data along q_z for pristine CsFAMA film and the CsFAMA film with AALs (OAm).

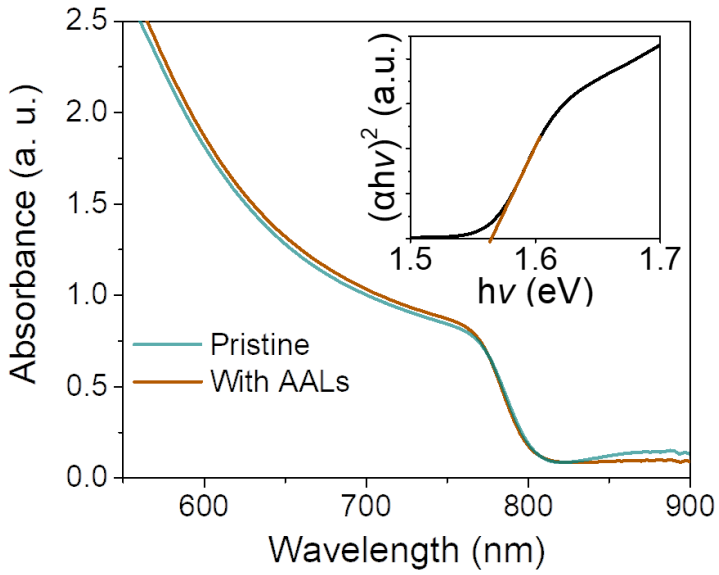

Supplementary Figure 4. UV-Vis spectrum and determination of optical band gap from intercept of Tauc plot. UV-Vis absorption spectra for the pristine CsFAMA film and the CsFAMA film with AALs (OAm). Inset is Tauc plot showing an optical bandgap of 1.56 eV for CsFAMA film.

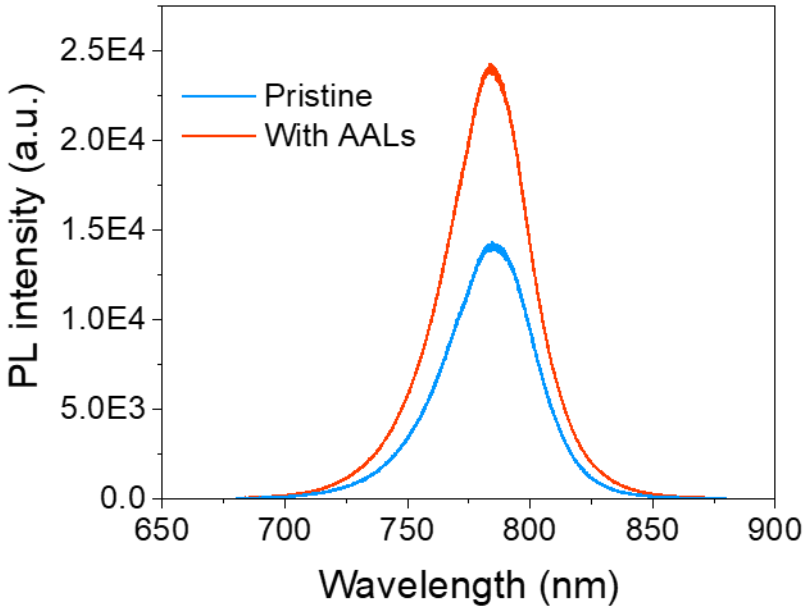

Supplementary Figure 5. Photoluminescence (PL) spectra of CsFAMA films with AALs. PL for pristine CsFAMA film and the CsFAMA film with AALs (OAm).

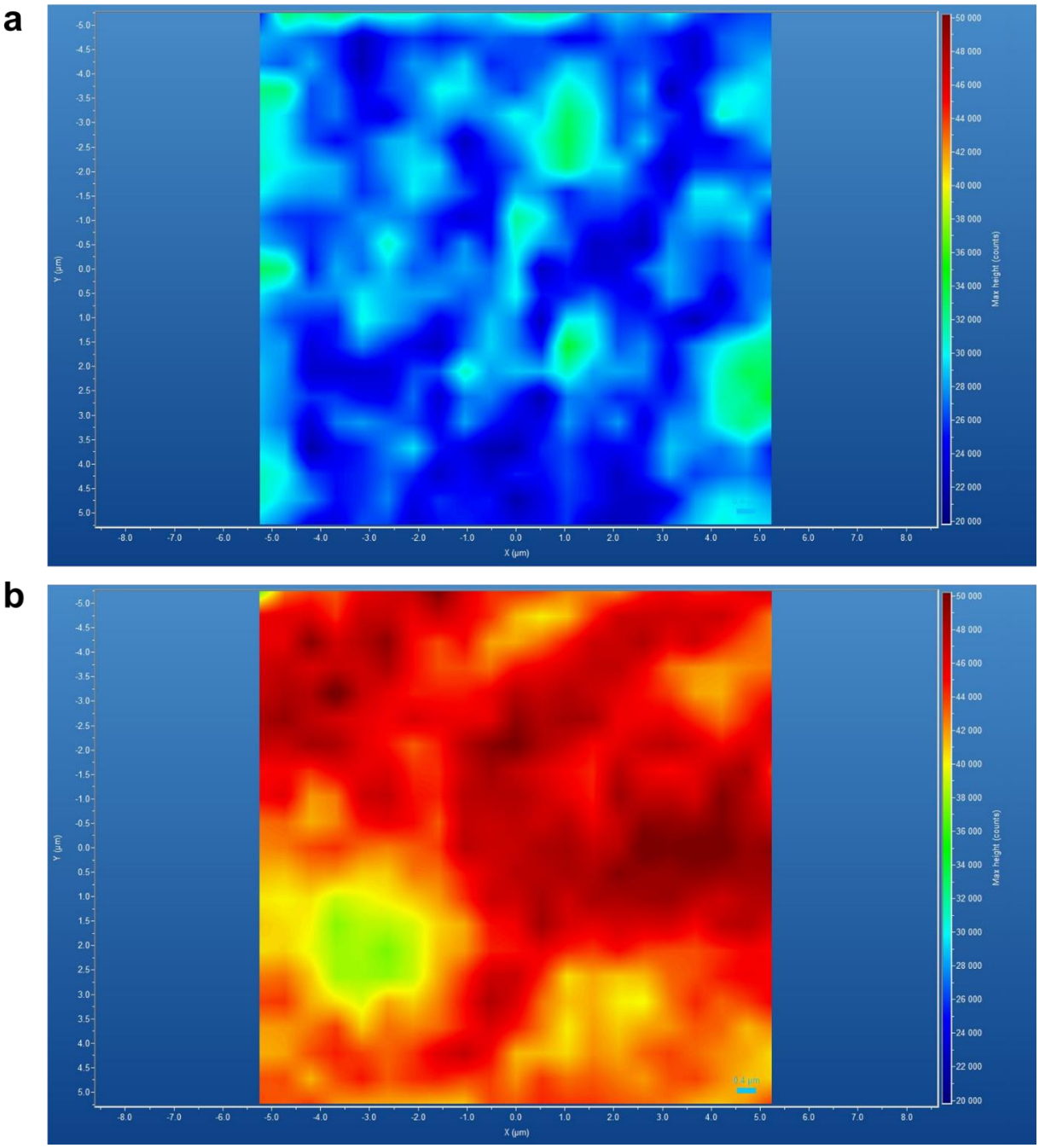

Supplementary Figure 6. Photoluminescence (PL) mapping of CsFAMA films with AALs. a and **b**, PL mapping for pristine CsFAMA film and the CsFAMA film with AALs (OAm), respectively.

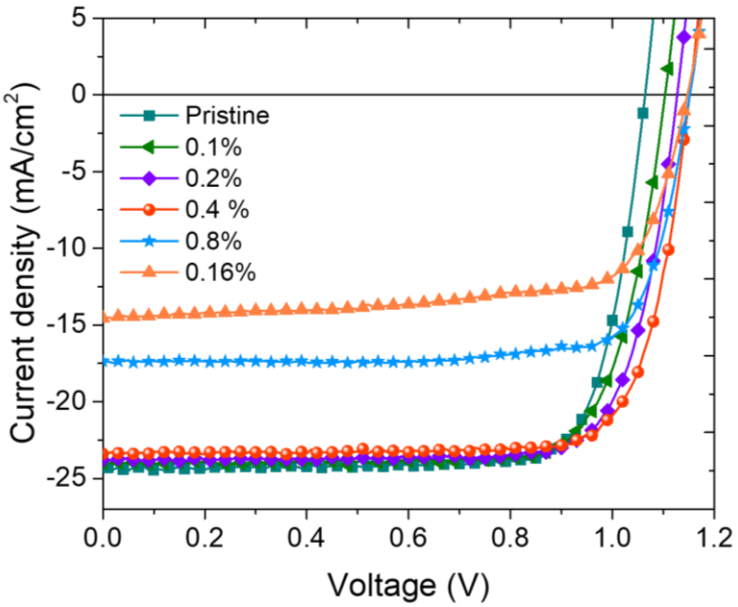

Supplementary Figure 7. **PEA concentration-dependent device *J-V* characteristics.** PEA concentration-dependent current density–voltage (*J-V*) characteristics of CsFAMA devices with PEA.

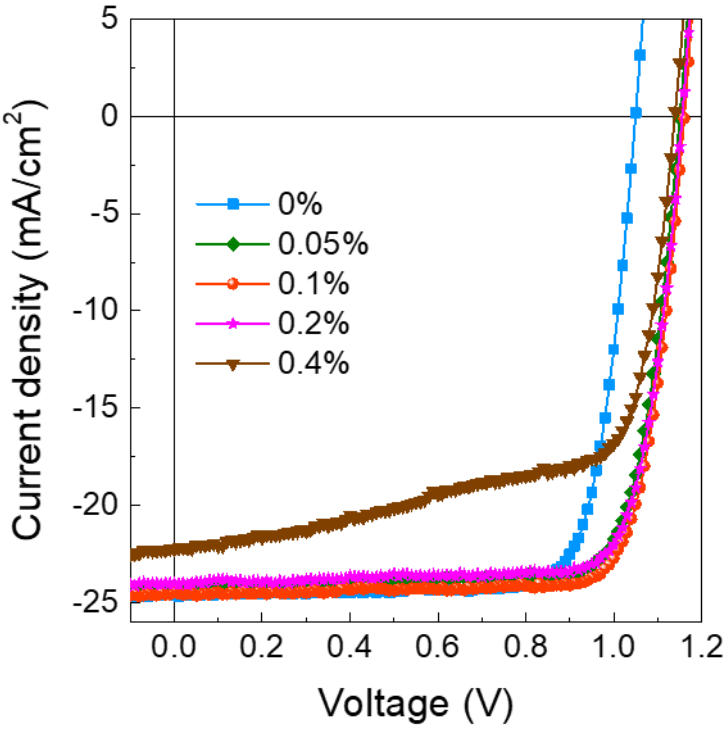

Supplementary Figure 8. OAm concentration dependent device performance. *J-V* characteristics of CsFAMA devices with different OAm concentrations.

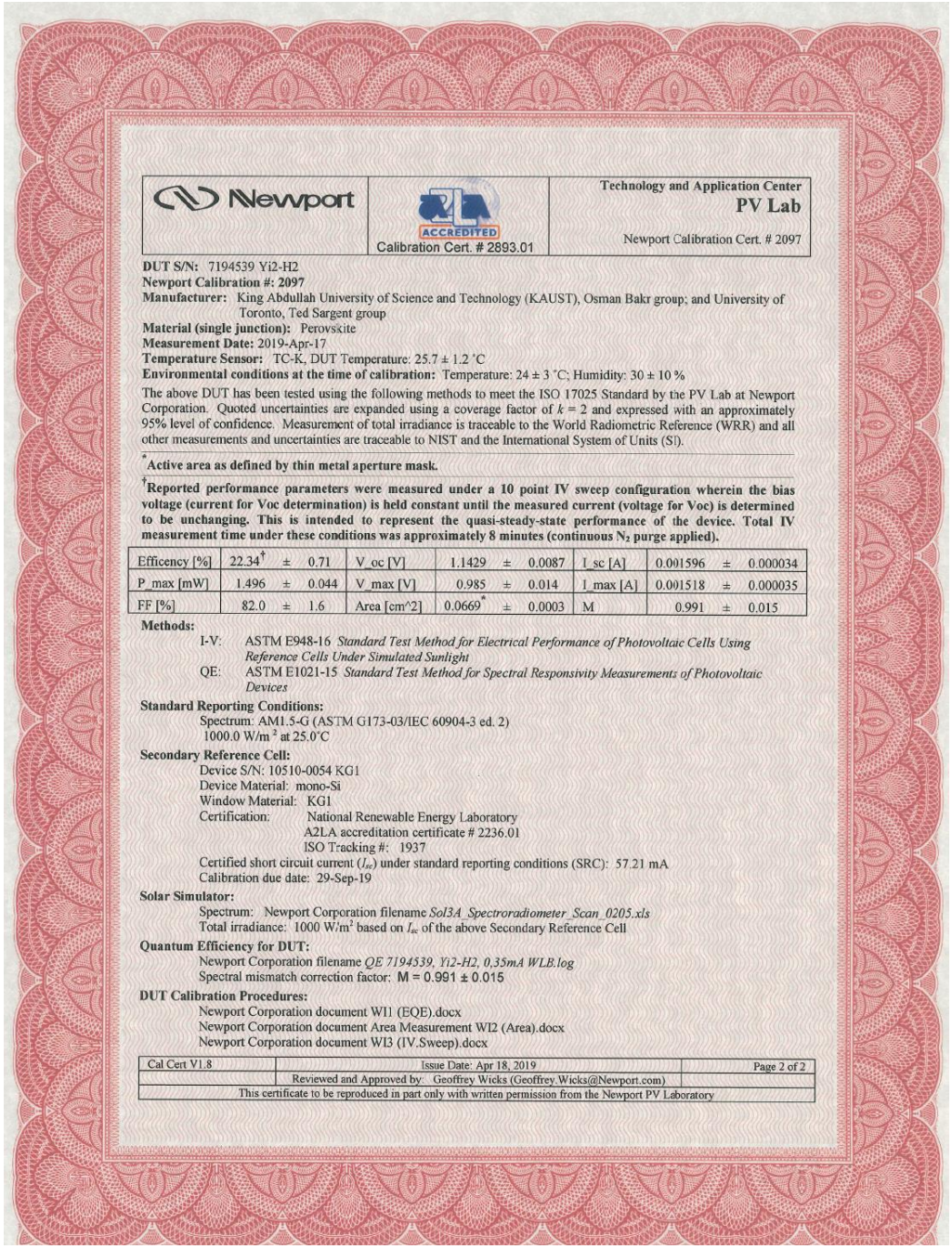

Newport

ACCREDITED
Calibration Cert. # 2893.01

Technology and Application Center
PV Lab
Newport Calibration Cert. # 2097

DUT S/N: 7194539 Yi2-H2
Newport Calibration #: 2097
Manufacturer: King Abdullah University of Science and Technology (KAUST), Osman Bakr group; and University of Toronto, Ted Sargent group
Material (single junction): Perovskite
Measurement Date: 2019-Apr-17
Temperature Sensor: TC-K, DUT Temperature: 25.7 ± 1.2 °C
Environmental conditions at the time of calibration: Temperature: 24 ± 3 °C; Humidity: 30 ± 10 %

The above DUT has been tested using the following methods to meet the ISO 17025 Standard by the PV Lab at Newport Corporation. Quoted uncertainties are expanded using a coverage factor of $k = 2$ and expressed with an approximately 95% level of confidence. Measurement of total irradiance is traceable to the World Radiometric Reference (WRR) and all other measurements and uncertainties are traceable to NIST and the International System of Units (SI).

*Active area as defined by thin metal aperture mask.

†Reported performance parameters were measured under a 10 point IV sweep configuration wherein the bias voltage (current for Voc determination) is held constant until the measured current (voltage for Voc) is determined to be unchanging. This is intended to represent the quasi-steady-state performance of the device. Total IV measurement time under these conditions was approximately 8 minutes (continuous N_2 purge applied).

Efficency [%]	22.34†	±	0.71	V_oc [V]	1.1429	±	0.0087	I_sc [A]	0.001596	±	0.000034
P_max [mW]	1.496	±	0.044	V_max [V]	0.985	±	0.014	I_max [A]	0.001518	±	0.000035
FF [%]	82.0	±	1.6	Area [cm^2]	0.0669*	±	0.0003	M	0.991	±	0.015

Methods:
I-V: ASTM E948-16 *Standard Test Method for Electrical Performance of Photovoltaic Cells Using Reference Cells Under Simulated Sunlight*
QE: ASTM E1021-15 *Standard Test Method for Spectral Responsivity Measurements of Photovoltaic Devices*

Standard Reporting Conditions:
Spectrum: AM1.5-G (ASTM G173-03/IEC 60904-3 ed. 2)
1000.0 W/m^2 at 25.0°C

Secondary Reference Cell:
Device S/N: 10510-0054 KG1
Device Material: mono-Si
Window Material: KG1
Certification: National Renewable Energy Laboratory
A2LA accreditation certificate # 2236.01
ISO Tracking #: 1937
Certified short circuit current (I_{sc}) under standard reporting conditions (SRC): 57.21 mA
Calibration due date: 29-Sep-19

Solar Simulator:
Spectrum: Newport Corporation filename *Sol3A_Spectroradiometer_Scan_0205.xls*
Total irradiance: 1000 W/m^2 based on I_{sc} of the above Secondary Reference Cell

Quantum Efficiency for DUT:
Newport Corporation filename *QE 7194539, Yi2-H2, 0,35mA WLB.log*
Spectral mismatch correction factor: M = 0.991 ± 0.015

DUT Calibration Procedures:
Newport Corporation document WI1 (EQE).docx
Newport Corporation document Area Measurement WI2 (Area).docx
Newport Corporation document WI3 (IV.Sweep).docx

Supplementary Figure 9. Device PCE certificate from Newport Photovoltaic Testing and Calibration Laboratory. Independent PCE certification of CsFAMA inverted perovskite solar cells with AALs (OAm) by an accredited laboratory (Newport Photovoltaic Testing and Calibration Laboratory in the U.S.), confirming a stabilized PCE of 22.34±0.71.

a

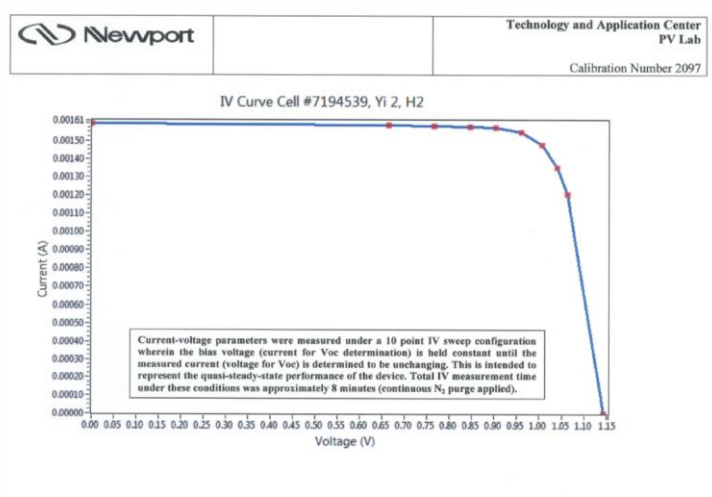

b

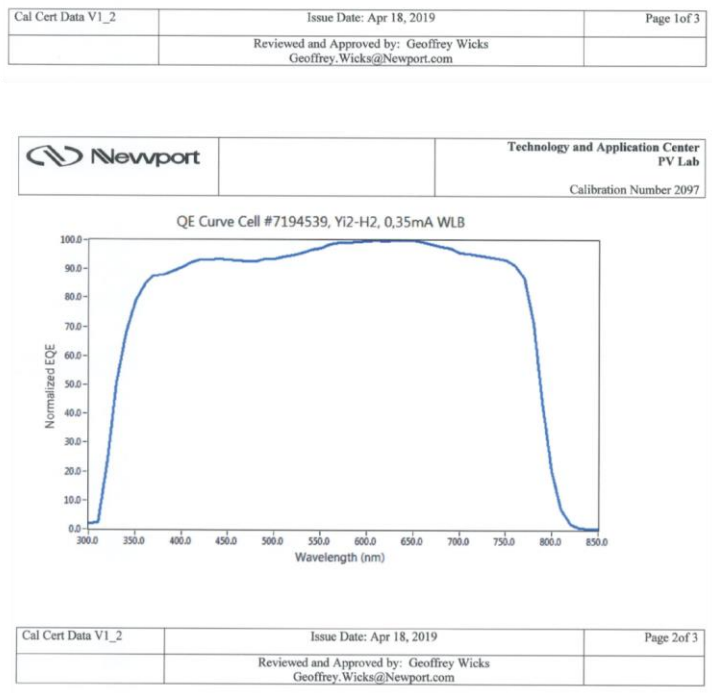

Supplementary Figure 10. Certificated results (*J-V* and EQE) by Newport Photovoltaic Testing and Calibration Laboratory. a, Quasi-steady-state (QSS) *J-V* characteristics of CsFAMA inverted perovskite solar cells with AALs (OAm) measured by Newport PV Lab under a 10 points *I-V* sweep protocol. 10 voltage points were collected in QSS measurement, and each bias voltage is applied and held until the measured current is determined to be unchanging. **b**, EQE of CsFAMA inverted perovskite solar cells with AALs (OAm) measured by Newport PV Lab.

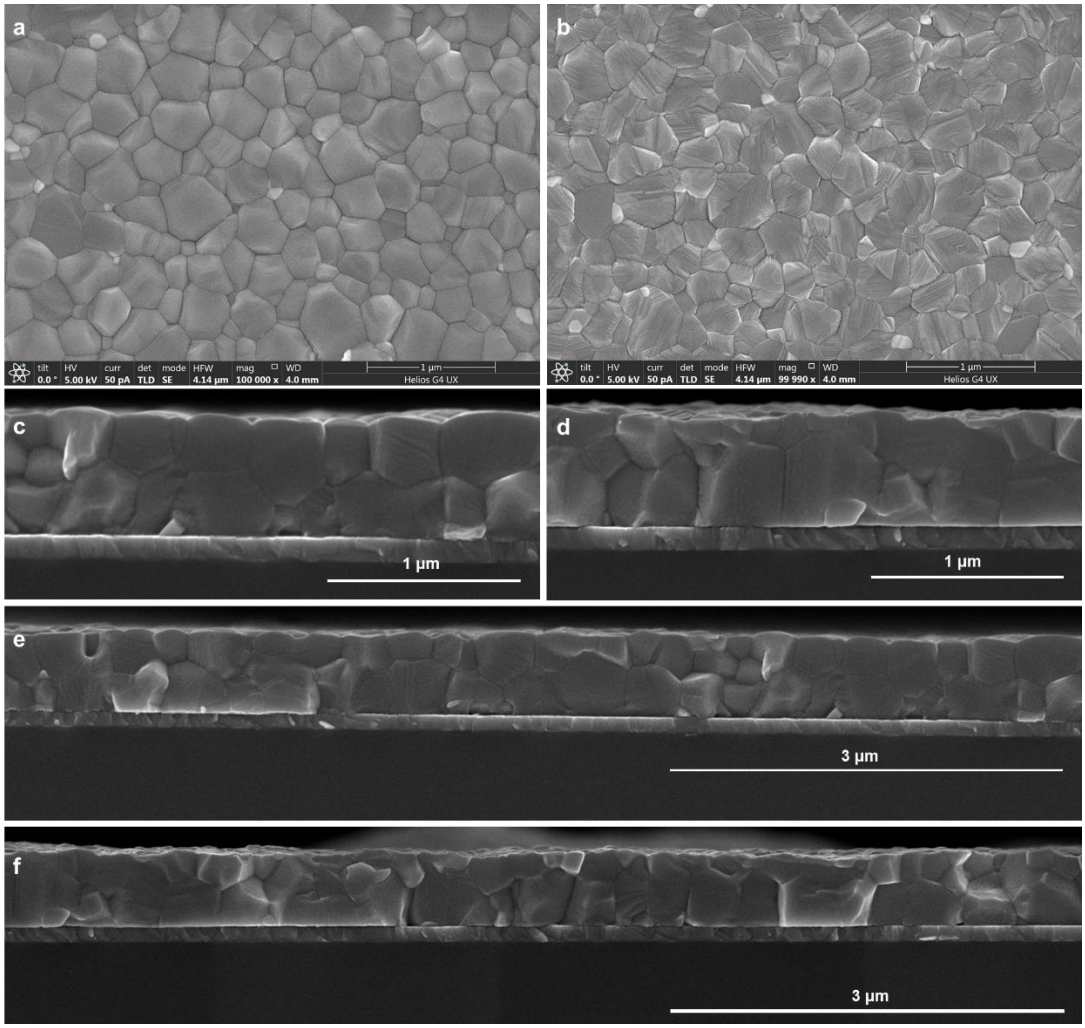

Supplementary Figure 11. Top-view and cross-sectional SEM images of CsFAMA films. a and **b**, Top-view SEM images of the pristine CsFAMA film and the CsFAMA film with AALs (OAm), respectively. **c** and **d**, Cross-sectional SEM images of the pristine CsFAMA film and the CsFAMA film with AALs (OAm), respectively. **e** and **f**, Large-scale cross-sectional SEM images of the pristine CsFAMA film and the CsFAMA film with AALs (OAm), respectively.

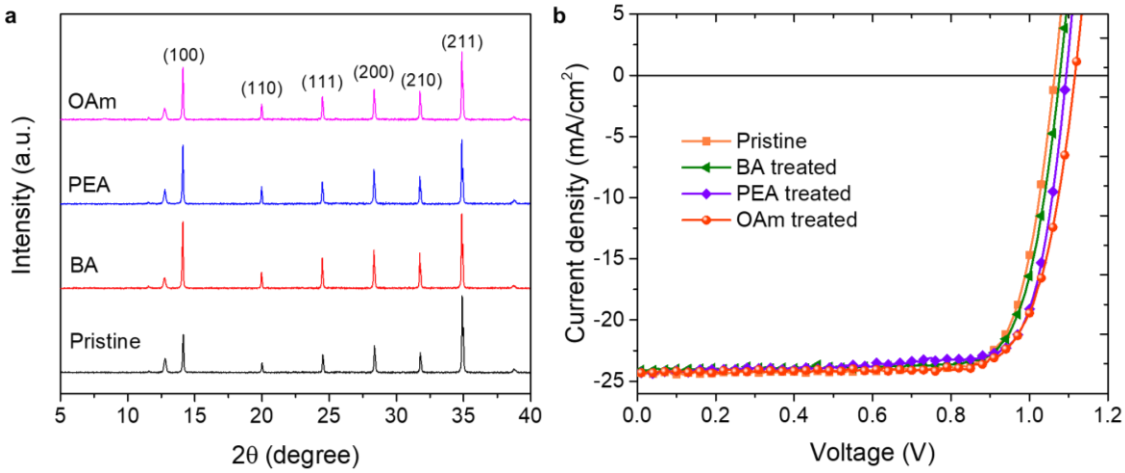

Supplementary Figure 12. **XRD patterns and device performance of CsFAMA perovskite with different alkyl chain length AAL surface post-treatment. a**, XRD patterns of CsFAMA perovskite films with different alkyl chain length AAL (BA, PEA, and OAm) post-treatment. **b**, Current density–voltage (*J*-*V*) characteristics of CsFAMA devices with different alkyl chain length AAL (BA, PEA, and OAm) post-treatment.

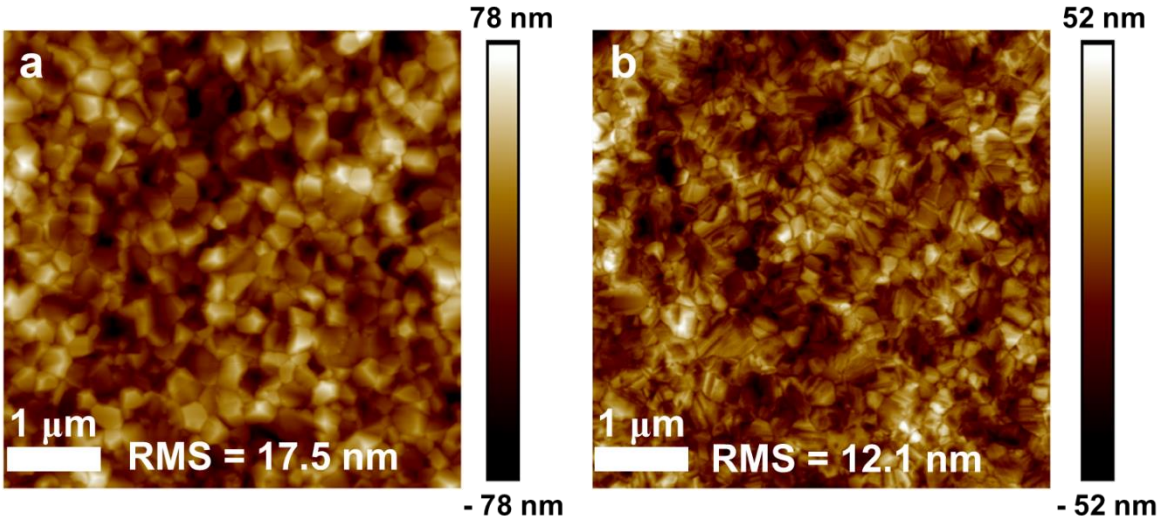

Supplementary Figure 13. Atomic force microscopy (AFM) images of CsFAMA films. a and **b**, Atomic force microscopy (AFM) images for pristine CsFAMA film and the CsFAMA film with AALs (OAm), respectively.

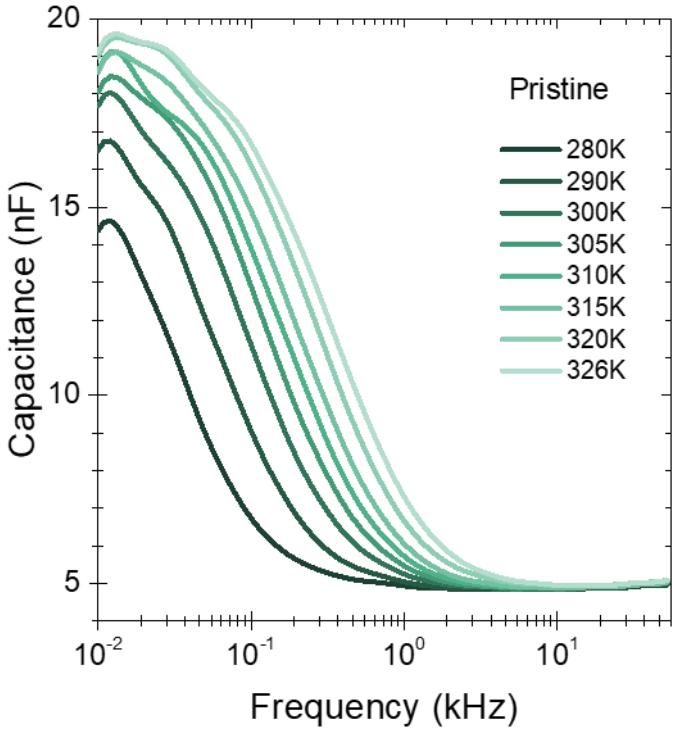

Supplementary Figure 14. Temperature-dependent capacitance versus frequency *C-f* plots.

Temperature dependent *C-f* plots for the pristine CsFAMA devices.

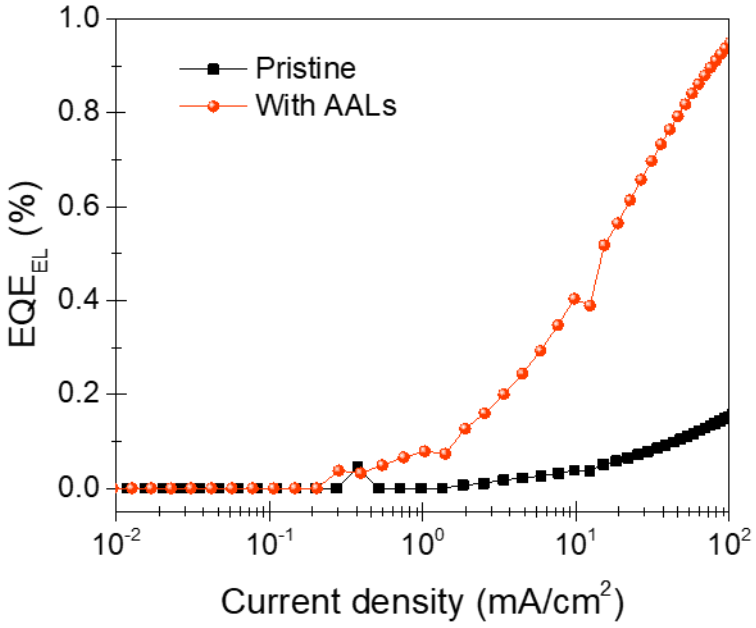

Supplementary Figure 15. EQE of the devices operated as LEDs. EQE_{EL} for pristine CsFAMA device and the CsFAMA device with AALs (OAm).

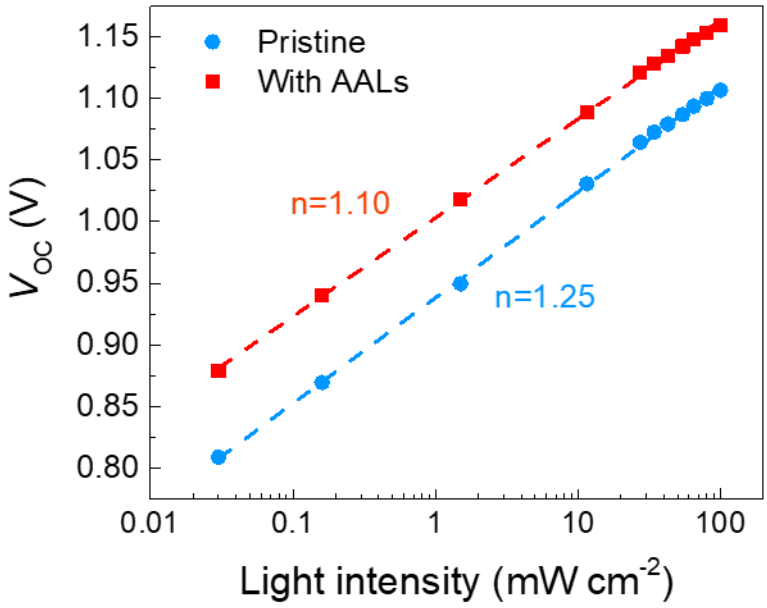

Supplementary Figure 16. Light intensity-dependent V_{OC} for CsFAMA devices. The light intensity-dependent V_{OC} for pristine CsFAMA device and the CsFAMA device with AALs (OAm). The *n* values were obtained by liner fitting of the data points.

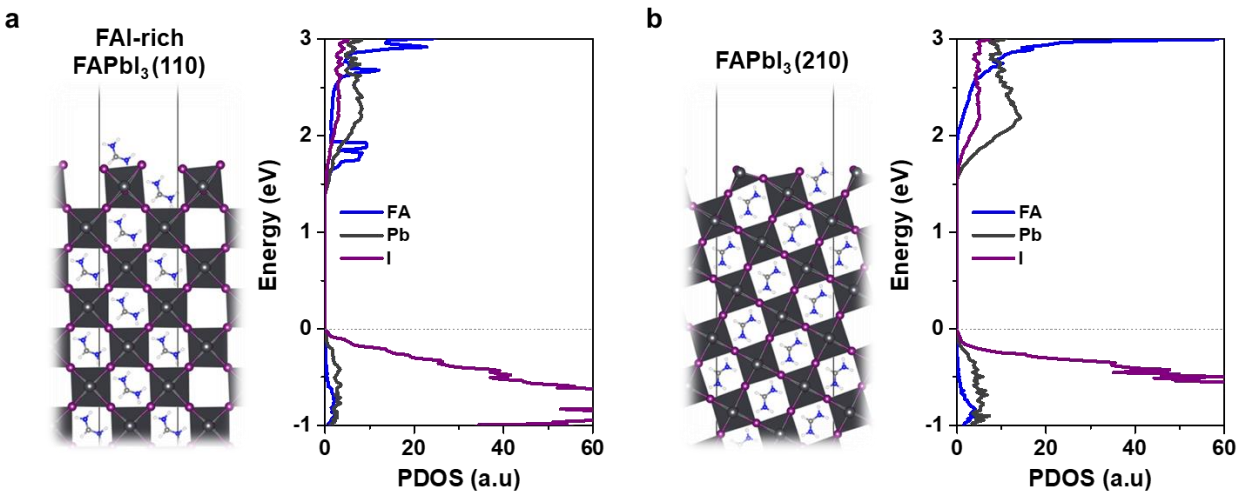

Supplementary Figure 17. DFT calculation of the trap states on the surface of (110) and (210) facet. Optimized crystal structures and projected density of states of cubic-phase $FAPbI_3$ slabs with surface facets: FAI-rich (110) (**a**) and (210) (**b**).

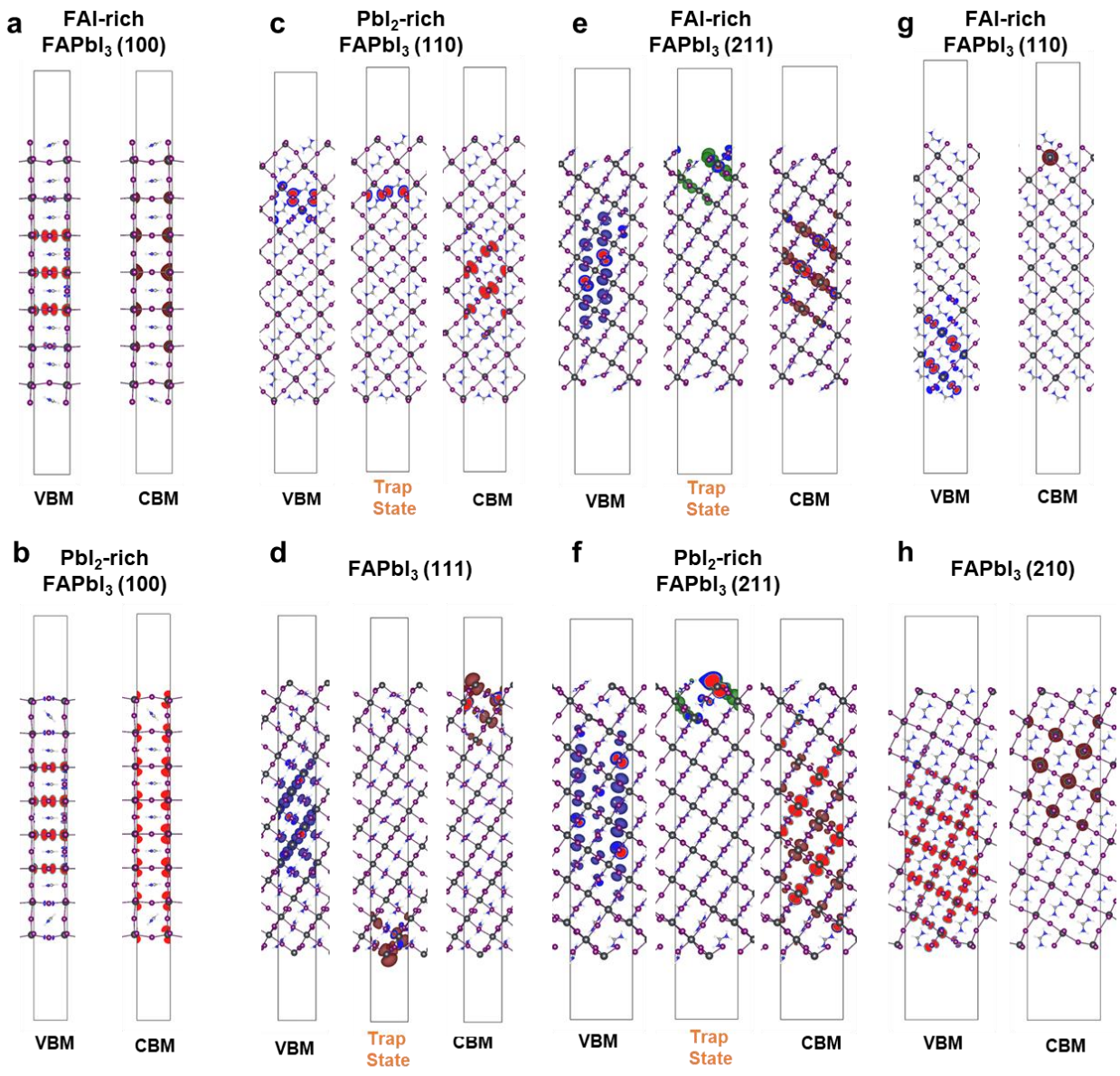

Supplementary Figure 18. DFT calculation of charge densities on the surface of various crystallographic facets. Charge densities for the valence band maximum (VBM), the conduction band minimum (CBM), and the trap states for cubic-phase $FAPbI_3$ slabs with surface facets: FAI-rich (**a**) and PbI_2-rich (**b**) (100), PbI_2-rich (110) (**c**), $FAPbI_3$ (111) (**d**), FAI-rich (**e**) and PbI_2-rich (**f**) (211), FAI-rich (110) (**g**), and $FAPbI_3$ (210) (**h**) calculated by density functional theory.

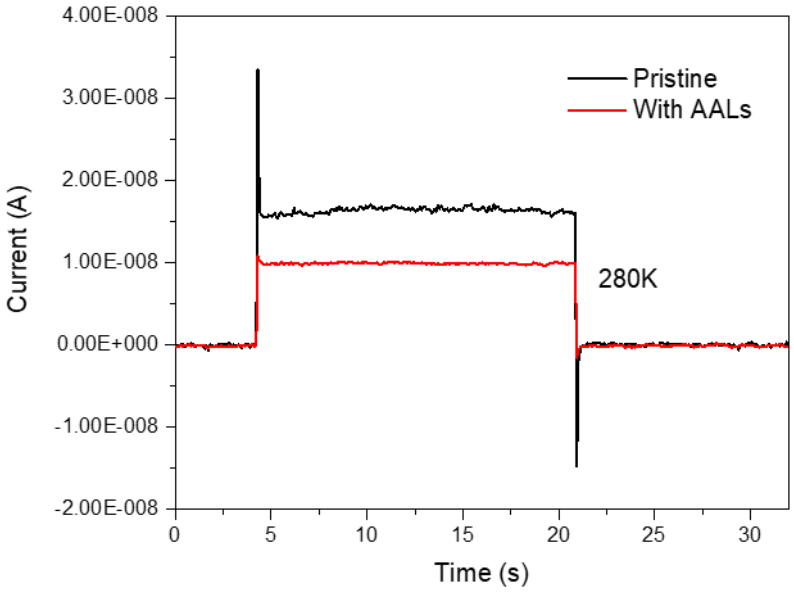

Supplementary Figure 19. Charging-discharging process of the ion migration measurement. A typical charging-discharging process for pristine CsFAMA film and the CsFAMA film with AALs (OAm) measured at 280 K.

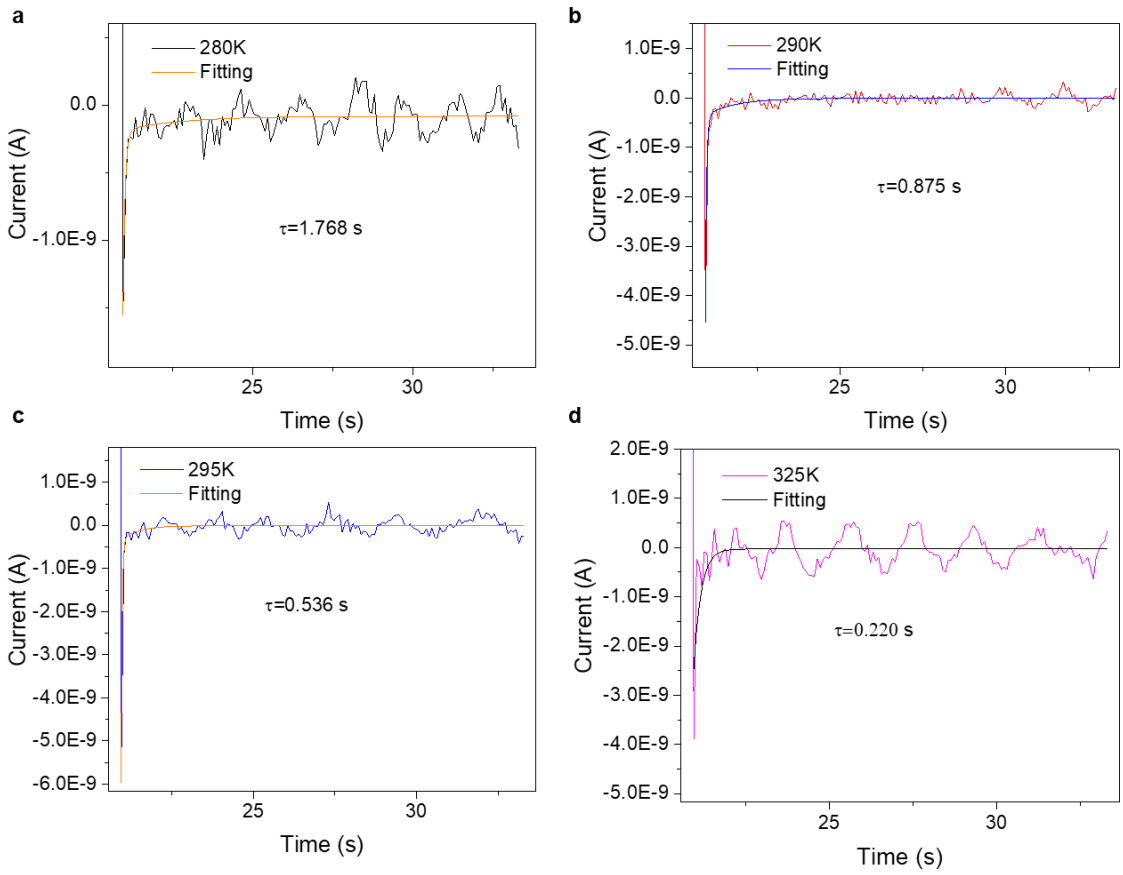

Supplementary Figure 20. Temperature-dependent transient response measurements for the ion migration characterization. Typical temperature-dependent transient response measurements for CsFAMA devices with AALs (OAm). The decay rate (τ^{-1}) of the negative current which represent the ion distribution recovery time, was estimated by exponential decay fitting.